

Phase Crossover induced by Dynamical Many Body Localization in Periodically Driven Long-Range Spin Systems

Mahbub Rahaman,¹ Takashi Mori,² and Analabha Roy¹

¹Department of Physics, The University of Burdwan, Golapbag, Bardhaman - 713 104, India

²RIKEN CEMS, 2-1 Hirosawa, Wako, Saitama, 351-0198, Japan

Dynamical many-body freezing occurs in periodic transverse field-driven integrable quantum spin systems. Under resonance conditions, quantum dynamics causes practically infinite hysteresis in the drive response, maintaining its starting value. We extended this to non-integrable many body systems by reducing the Hamiltonian symmetries through a power-law dependence in spin exchange energy, $J_{ij} = 1/|i - j|^\beta$. The dynamics of the integrable short-range Transverse Field Ising Model (TFIM) and non-integrable long-range Lipkin Meshkov-Glick (LMG) models were investigated. In the LMG, the resonance conditions in the driving field suppresses the heating postulated by the *Eigenstate Thermalization Hypothesis* (ETH) by inducing *Dynamical Many Body Localization*, or DMBL. This is in contrast to Many Body Localization (MBL), which requires disorder to suppress ETH. DMBL has been validated by the Inverse Participation Ratio (IPR) of the quasi-stationary Floquet modes. While TFIM has IPR localization for all drive parameters, the LMG exhibits high-frequency localization only at the resonances. IPR localization in the LMG deteriorates with an inverse system size law at lower frequencies, which indicates heating to infinite temperature. Furthermore, adiabatically increasing frequency and amplitude from low values raises the Floquet state IPR in the LMG from nearly zero to unity, indicating a phase crossover. This occurrence enables a future technique to construct an MBL engine in clean systems that can be cycled by adjusting drive parameters only.

Keywords: Dynamical localization, Thermalization, Phase Crossover

Periodically driven Quantum Many Body Systems should experience Dynamical Freezing (DMF) when dynamical hysteresis stops observables from reaching their diagonal averaged values and thermalizing to infinite temperature [1–3]. Under certain resonance conditions in the drive parameters, DMF can cause the response to ‘freeze’ completely to its initial value at all times. This arises as a consequence of additional approximate symmetries that occur at resonance. DMF has been demonstrated via the Rotating Wave Approximation (RWA) in the driven TFIM with nearest neighbour interactions [4] and is shown to be protected when translational invariance is explicitly broken (say, by disorder) [5, 6].

The utilization of Floquet theory simplifies the analysis of time-periodic systems. For closed quantum systems governed by the time-dependent Schrödinger equation, the *Floquet Hamiltonian* allows for a mapping of the time-dependent dynamics into the dynamics of a time-independent effective Hamiltonian, provided the system is strobed at integer multiples of the time period of the drive. The time independent eigenstates of the effective Hamiltonian correspond to quasi-stationary *Floquet Modes* of the original Hamiltonian. The temporal progression of the system comes from phase coefficients that capture the dynamics [7, 8].

Any sufficiently complex non-integrable Many Body System is expected to thermalize according to the Eigenstate Thermalization Hypothesis (ETH) despite

the fact that closed quantum dynamics preserves the memory of the initial state of the system. This arises due to the properties of the matrix elements of observables in typical states[9]. The ETH can be readily adapted to time-periodic systems using Floquet theory (the Floquet-ETH, or FETH). Nonetheless, the conditions for ETH to hold are not particularly strong, and the density matrix of the system can fail to approach one that is described by a thermal expression. In such cases, the system is said to undergo *Many Body Localization* (MBL)[10]. This phenomenon is stable against local perturbations, and constitutes an exotic state of matter with far-reaching implications in theoretical physics, as well as in practical applications[11].

The addition of disorder has been identified as a crucial component in the onset of MBL. In that case, thermalization is prevented by disorder-induced localization. An alternative approach to realizing MBL in clean many-body system involves *Floquet Engineering*, where a time-periodic drive is introduced, and the drive parameters tuned so as to introduce a clustering of quasistationary energies in a manner similar to localization[9].

In this article, we propose that additional approximate symmetries can be Floquet-engineered in quantum many body systems with lower symmetry than the TFIM, such as those with long-range interactions. This results in both DMF and MBL occurring simultaneously at resonant values of the drive parameters, and complete thermal behaviour at other values. This

68 phenomenon is distinct from DMF in the TFIM, since 120
 69 clean TFIM systems, being integrable, never thermal-
 70 ize.

71 To demonstrate the onset of MBL, we investigate 121
 72 the driven Lipkin-Meshkov-Glick (LMG) model, a long-
 73 range system that is a special case of the more general
 74 Curie-Weiss model, wherein the nearest-neighbour ex-
 75 change in the TFIM is extended to longer ranges with
 76 a power law dependence, $J_{ij} \sim 1/|i - j|^\beta$ [12-14].
 77 Setting $\beta = \infty$ recovers the TFIM, and setting $\beta = 0$
 78 yields the LMG model. We have recovered the onset
 79 of DMF in this system and have supported our result
 80 with numerical simulations.

81 In addition, we compare the degree of localization 122
 82 of the quasi-stationary Floquet modes in both limits of
 83 β . In order to do so, we look at the Inverse Partici-
 84 pation Ratio (IPR) of the Floquet modes in the repre-
 85 sentation given by the eigenstates of the symmetry-
 86 breaking field. The IPR, closely related to the concept
 87 of quantum purity, is defined as the formal sum of the
 88 square of the density in some physically meaningful
 89 space or representation. A high IPR of a stationary
 90 state denotes low participation in most of the repre-
 91 sentation, and a low IPR distributes participation uni-
 92 formly across the representation, leading to ergodic
 93 dynamics[15]. Thus, IPR [16] is a useful tool for wit-
 94 nessing MBL of a quantum system. For an MBL sys-
 95 tem, the IPR is unity, and it scales inversely with the
 96 system size when it is thermally distributed [17].

97 In the first section of this paper, we present all es-
 98 sential theoretical frameworks. Our results for the
 99 LMG model are presented next in section II. In that
 100 section, we have used the Rotating Wave Approx-
 101 imation (RWA) [18], where only the slowest rotating
 102 terms in the Fourier expansion of the Hamiltonian in
 103 a frame co-rotating with the symmetry breaking drive
 104 field are retained. In addition, we have the obtained
 105 analytical expressions for the Floquet modes and their
 106 IPR. They are used to probe the system dynamics in
 107 the high and low-frequency domains at both limits of
 108 β . In section III we have used phase space plots to
 109 contrast the low and high frequency limits of the LMG
 110 model in the thermodynamic limit by mapping it to an
 111 equivalent classical Hamiltonian system. Finally, in
 112 section IV, we have looked at numerical computations
 113 of the IPR of the Floquet modes for different values of
 114 the drive parameters, well beyond those that allow for
 115 the RWA. We observed that, if the system is driven by
 116 an adiabatically increasing drive frequency from low
 117 to high limit while remaining in the resonance region,
 118 a sharp crossover from a thermal to an MBL phase
 119 occurs. We conclude with discussions and outlook.

I. BACKGROUND

121 The Eigenstate Thermalization Hypothesis (ETH) is
 122 a series of conjectures that allows for the thermaliza-
 123 tion of an isolated quantum many body system. The
 124 state of the system, $|\psi(t)\rangle$, evolves according to the
 125 Schrödinger equation $\hat{H}|\psi(t)\rangle = i\frac{\partial}{\partial t}|\psi\rangle$. The Hamilto-
 126 nian \hat{H} is assumed to be *non-integrable*, in that it lacks
 127 an extensive number of *local* additive conserved quan-
 128 tities, that is to say, there are no set of observables
 129 \hat{O}_s such that $\hat{H} = \sum_s \hat{O}_s$ for any extensive index s .
 130 Here, the \hat{O}_s constitute an arbitrary CSCO (complete
 131 set of commuting observables) that are *local*, having
 132 sub-extensive support in the system size. In addition,
 133 we postulate the existence of an equivalent Hamilto-
 134 nian \hat{H}_{eq} for every Hamiltonian \hat{H} as well as an "equi-
 135 librium" value A_{eq} for every observable \hat{A} , such that

$$A_{eq}(E) \equiv \frac{\text{Tr}(\hat{A}e^{-\beta\hat{H}_{eq}})}{\text{Tr}(e^{-\beta\hat{H}_{eq}})}. \quad (1)$$

136 where $E = \langle\psi(t)|\hat{H}|\psi(t)\rangle$ is the conserved energy of
 137 the system, and $\beta = 1/(k_B T)$ is the inverse tempera-
 138 ture, H_{eq} is an effective Hamiltonian that captures the
 139 long-time average dynamics of the system, and k_B is
 140 the Boltzmann constant.

To put it simply, ETH proposes that this many-
 body Hamiltonian undergoes thermalization as seen
 in the *long-time averages* of observables, with the
 eigenstates bearing resemblance to thermal states.
 The aforementioned hypothesis serves as a valuable
 instrument for comprehending the conduct of stim-
 ulated quantum systems and their correlation with
 thermal equilibrium. This assertion can be justified
 by examining the expectation value of an observable
 \hat{A} as it evolves under the Schrödinger equation. To
 see this, we first expand the state of the system $|\psi(t)\rangle$
 as:

$$|\psi(t)\rangle = \sum_m c_m(t) |m(0)\rangle,$$

141 where $|m(0)\rangle$ represents the eigenstates of $\hat{H}(0)$ with
 142 energy E_m . The coefficients $c_m(t)$ describe the time-
 143 dependent amplitude of the expansion. Plugging
 144 these expansions into the expression for the expec-
 145 tation value, we obtain the long-time average of the
 146 expectation value [19]:

$$\overline{\langle \hat{A}(t) \rangle} = \sum_{m,k} \overline{c_m^*(t)c_k(t)} \langle m(0)|\hat{A}|k(0)\rangle, \quad (2)$$

147 where the overline indicates the following operation
 148 for any time-dependent quantity $\mathcal{O}(t)$,

$$\overline{\mathcal{O}} \equiv \lim_{T \rightarrow \infty} \frac{1}{T} \int_0^T dt \mathcal{O}(t). \quad (3)$$

Had the system been integrable, the large number of conserved quantities would restrict mixing between the states during unitary evolution. In the non-integrable case, the system explores the entire Hilbert space spanned by eigenstates with eigenvalues close to E more-or-less uniformly. In that case, the matrix elements $\langle m(0)|\hat{A}|k(0)\rangle$ are said to satisfy the Srednicki ansatz [20, 21]:

$$\langle m(0)|\hat{A}|k(0)\rangle \approx A_{eq} \left(\frac{E_m + E_k}{2} \right) \delta_{mk} + e^{-\frac{1}{2}S\left(\frac{E_m+E_k}{2}\right)} f\left(\frac{E_m + E_k}{2}, E_m - E_k\right) R_{mk}. \quad (4)$$

Here, S is the thermodynamic entropy and R_{mk} are elements of a random matrix with vanishing mean and unit variance. What this means for the ensuing dynamics is that the system explores the accessible Hilbert space uniformly, and the matrix elements $\langle m(0)|\hat{A}(t)|k(0)\rangle$ become indistinguishable for most pairs of m and k . Applying this ansatz and taking the thermodynamic limit by ignoring terms $\mathcal{O}(e^{-S/2})$, the expression for the expectation value becomes:

$$\overline{\langle \hat{A}(t) \rangle} \approx \sum_m \overline{|c_m(t)|^2} A_{eq} \left(\frac{E_m + E_k}{2} \right) \approx A_{eq}(E) \sum_m \overline{|c_m(t)|^2} = A_{eq}(E),$$

where, in the last step, we utilized the fact that A_{eq} is a smooth function, and that the states with energies far from E have $|c_m(t)|^2 \approx 0$. Therefore, in the limit of large systems the expectation value of an observable \hat{A} is approximately equal to the thermal expectation value A_{eq} . This is the essence of the ETH, which suggests that individual eigenstates of a quantum system can be described by statistical mechanics in the long-time limit.

We now generalize the ETH to non-integrable many-body systems that are closed, but not isolated. In that case, it is possible to impart a periodic time-dependence on the Hamiltonian while still ensuring unitary evolution. If the time period of the drive is T , and the corresponding drive frequency $\omega \equiv 2\pi/T$, the Floquet theorem states that the solutions to the Schrödinger equation can be written as $|\psi(t)\rangle = e^{-i\epsilon t/\hbar} |\phi(t)\rangle$, where the $|\phi(t)\rangle$ are T -periodic states called *Floquet Modes*, the corresponding $\epsilon \in \mathbb{R}$, are called *quasienergies*. Quasienergy values are not unique, and can be made to be bounded within a Floquet photon, viz. a range $[-\omega/2, \omega/2]$ [22, 23]. As a consequence, the unitary evolution operator can be split into two parts as follows [24].

$$U(t) = e^{-i\hat{K}_F(t)} e^{-i\hat{H}_F t}. \quad (5)$$

Here, the micromotion operator $\hat{K}_F(t)$ is time-periodic in T , with $\hat{K}_F(0) = 0$, and the Floquet Hamiltonian $\hat{H}_F = \hat{H}(t) - i\frac{\partial}{\partial t}\Big|_{t=T}$. Thus, if the system is strobed at integer multiples of T only, then the unitary evolution matches that of a time independent Hamiltonian H_F . This can capture most of the exact dynamics at large frequencies.

In such systems, the Floquet Eigenstate Thermalization Hypothesis (FETH) posits that, subject to specific conditions and in the context of a system of significant size, the Floquet modes themselves exhibit thermal state-like behavior, i.e., $\hat{H}_{eq} \approx \hat{H}_F$ in eqn 1. However, in contrast to the isolated systems, the loss of energy conservation allows for the mixing of all Floquet modes in the ensuing dynamics, not just those with quasienergies near E . Were this to actually happen in the ensuing dynamics, it can be reconciled with ETH [25] by ensuring that $\beta = 0$ in eq 1. In other words, the nonequilibrium steady state of the system tends to an infinite temperature, maximum entropy density matrix.

However, drive parameters like amplitude, frequency, and duty-cycle strongly affect the structure of the Floquet modes $|\phi\rangle$. Thus, they can be engineered to prevent the kind of full mixing that would lead to infinite temperatures, manifesting suppression of thermalization dynamically. Thus, this type of *Floquet Engineering* can produce *Dynamical Many Body Localization* (DMLB), where the system fails to reach thermal equilibrium and remains localised, possibly near its initial state, even at large times. This paradigm seems similar to standard Many-Body Localization [26, 27], where disorder, locality, and integrability can cause athermalism via breakdown in the Srednicki ansatz. However, DMLB is a purely dynamical phenomenon, and thus can occur regardless of disorder, locality of observables, or system integrability, all of which have been studied for MBL onset [28–30].

Integrable Many Body systems do not exhibit thermalization. When subjected to time-periodic drives, Floquet engineering allows for the introduction of additional approximate conserved quantities that dynamically suppress the evolution of certain observables by hysteresis. This type of *freezing* of response has been shown in integrable systems [6]. A paradigmatic example is the driven Transverse Field Ising model (TFIM) in one dimension [31]. The Hamiltonian

is given by

$$\hat{H}(t) = \hat{H}_0 + h_z(t) \hat{H}_1 \quad (6)$$

$$\hat{H}_0 = -\frac{1}{2} \sum_{i=1}^N \sigma_i^x \sigma_{i+1}^x \quad (7)$$

$$\hat{H}_1 = -\frac{1}{2} \sum_{i=1}^N \sigma_i^z. \quad (8)$$

Here, the undriven Hamiltonian \hat{H}_0 consists of nearest-neighbour interactions between N number of spin-1/2 particles on a one-dimensional spin network. The transverse field is denoted by \hat{H}_1 , and is being varied by a time-periodic and harmonic signal $h_z(t) = h_0 + h \cos \omega t$, yielding a time period $T = 2\pi/\omega$ with amplitude h , drive frequency ω , and d.c. field h_0 . This Hamiltonian can be readily transformed into a spinless pseudo-fermionic system via the Jordan-Wigner transformation [4]. When written in momentum space spanned by spinors $\psi_k = (c_{-k}, c_k^\dagger)^T$ of fermions at momentum k created (annihilated) by operators c_k^\dagger (c_k), the effective Hamiltonian

$$H(t) = \sum_{(k,-k)-\text{pairs}} \psi_k^\dagger \left[\left(f_k - h_z(t) \right) \tau_z + \tau_x \Delta_k \right] \psi_k \quad (9)$$

with $f_k = J \cos k$, $\Delta_k = J \sin k$, τ_{xyz} are the three Pauli Matrices, and the sum is over distinct $(k, -k)$ Cooper Pairs. We can transform our system to a frame that rotates with the time-varying symmetry-breaking field. This is achieved by the means of the unitary transformation operator

$$U(t) = \prod_k U_k(t) \quad (10)$$

$$U_k(t) = \exp \left\{ \left[\frac{i\hbar}{\omega} \sin \omega t \right] \tau_z \right\}.$$

The resulting transformed Hamiltonian $H'(t) = U^\dagger(t) H(t) U(t) - iU^\dagger(t) \partial_t U(t)$ simplifies to

$$H'(t) = \sum_{(k,-k)-\text{pairs}} \psi_k^\dagger \left[\tau_z f_k + \tau_x \cos(\eta \sin \omega t) + \tau_y \sin(\eta \sin \omega t) \right] \psi_k, \quad (11)$$

where we defined $\eta = 2h/\omega$. Using the Jacobi-Anger formula [32]

$$e^{i\eta \sin \omega t} = \sum_{n=-\infty}^{\infty} J_n(\eta) e^{in\omega t}, \quad (12)$$

where $J_n(\eta)$ are Bessel Functions, the transformed Hamiltonian simplifies to

$$H'(t) = \sum_{(k,-k)-\text{pairs}} \psi_k^\dagger \left\{ \tau_z f_k + 2\tau_x \Delta_k \sum_{n \geq 0} J_{2n}(\eta) \cos(2n\omega t) - 2\tau_y \Delta_k \sum_{n \geq 0} J_{2n+1}(\eta) \sin[(2n+1)\omega t] \right\} \psi_k, \quad (13)$$

In the frequency regime $\omega \gg f_k$, the long-time average $H^{RWA} \equiv \lim_{n \rightarrow \infty} \frac{1}{nT} \int_0^{nT} dt H'(t)$ can serve as a suitable approximation for $H'(t)$. This approximation, known as the *Rotated Wave Approximation* (RWA), eliminates the oscillating modes and results in an effective Hamiltonian that is independent of time.

$$H^{RWA} = \sum_{(k,-k)-\text{pairs}} \psi_k^\dagger \left[f_k \tau_z + 2J_0(\eta) \Delta_k \tau_x \right] \psi_k, \quad (14)$$

It is evident that by manipulating the drive parameters, specifically the amplitude denoted by h and the frequency denoted by ω , in a manner such that η is positioned on a root of $J_0(\eta)$, the fermion number can be conserved to a significant extent at this particular resonance. Consequently, it is feasible to exercise direct control over H^{RWA} , resulting in a comprehensive suppression of the dynamics of otherwise responsive observables.

This phenomenon is highly general in nature, and can be readily adapted to non-integrable systems. In such cases, freezing has the additional effect of inducing DMBL, suppressing thermalization to infinite temperatures. Numerical quantification of localization of a specific (quasi) stationary state in a physically significant representation can be achieved through the computation of the *Inverse Participation Ratio* (IPR). In the position representation, the IPR for a state $|\psi\rangle$ [33-36] is defined as

$$\phi_{IPR} \equiv \int dx |\langle x | \psi \rangle|^4$$

This definition can be generalized to the IPR of a state $|\phi\rangle$ in a representation given by complete orthonormal basis $|m\rangle$ as

$$\phi_{IPR} \equiv \sum_m |\langle m | \psi \rangle|^4. \quad (15)$$

The smallest value of the IPR corresponds to a fully delocalized state, $\psi(x) = 1/\sqrt{N}$ for a system of size N [36, 37]. Values of the IPR close to unity correspond to localized states [38]. For a periodically driven system, we look at the IPR of the quasi-stationary Floquet modes at $t = T$, where $t = 2\pi/\omega$ for drive frequency ω .

251 In the TFIM model, equation 14 indicates that, at reso-
 252 nance, when $J_0(\eta) = 0$, the Floquet modes are approx-
 253 imately given by the fermionic Fock states, which have
 254 a trivially unit IPR in the representation of the eigen-
 255 modes of the transverse field \hat{H}_1 in equation 6. Here, a
 256 particular Floquet mode can be decomposed into a di-
 257 rect product of cooper-pair states as $|\phi\rangle = \prod_{k,-k} |\phi_k^n\rangle$.
 258 In the RWA limit and at resonance, $|\phi_k^n\rangle$ has values of
 259 $|0\rangle, |k, -k\rangle$ for two values of $n = 0, 1$ respectively. We
 260 define the reduced IPR of $|\phi_k^n\rangle \forall k$ to be

$$\phi_{IPR}^{(n)}(k) = |\langle 0|\phi_k^n\rangle|^4 + |\langle +k, -k|\phi_k^n\rangle|^4, \quad (16)$$

261 where $n = 0, 1$. In the RWA limit and at resonance
 262 , this quantity is unity, indicating very low participa-
 263 tion and the onset of freezing. Figure 1 shows results

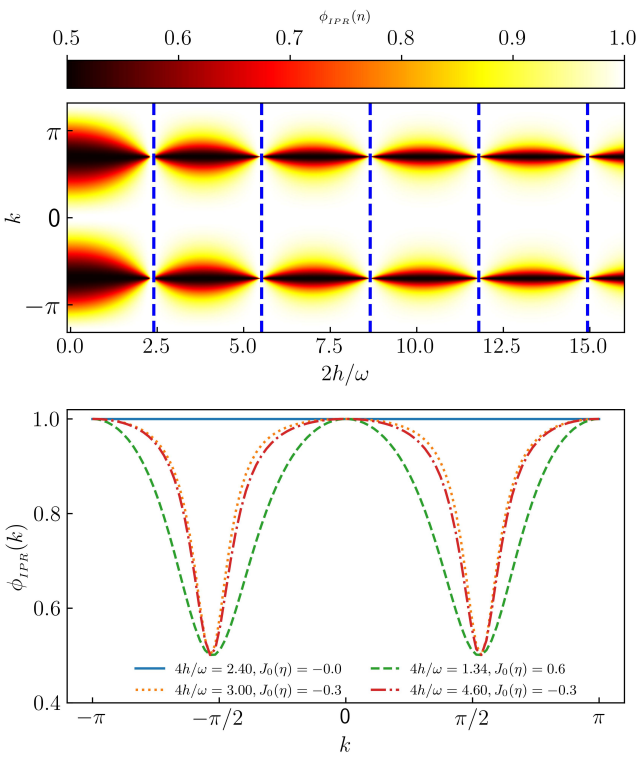


FIG. 1. Reduced IPR (defined in equation 16) for one of the two Floquet modes obtained from the exact dynamics of the TFIM for size $N = 100$ and $\omega = 90$ for the entire Brillouin zone (top panel, ordinate) and a few drive amplitudes (top panel, abscissa). The dashed lines (top panel) indicate the roots of $J_0(\eta)$. The bottom panel shows cross-sections for four different chosen amplitudes.

264 from numerically simulating the TFIM dynamics. The
 265 reduced IPR for a particular Floquet mode recovered
 266 by simulating the exact Schrödinger dynamics over a
 267 single time period of the drive, and plotted as a func-
 268 tion of momentum k for different η 's. At resonance,
 269 when η lies at the root of the Bessel function $J_0(\eta)$,

270 the IPR is exactly unity for all momenta. Outside this
 271 resonance, the IPR is unity only for some momenta
 272 because the effective Hamiltonian is perfect diagonal
 273 at $k \in \{-\pi, 0, \pi\}$ as can be seen in the cross-sectional
 274 plots of figure 1. As we move away from the resonance
 275 point, IPR reduces from unity. However, as the TFIM
 276 is an integrable spin model, the IPR never drops to a
 277 value that is small enough to indicate thermalization.
 278 At low frequencies, RWA fails due to the unavailability
 279 of zero off-diagonal terms in the effective transformed
 280 Hamiltonian, as well as the absence of integrability
 281 breaking terms to counteract the off diagonal terms.
 282 Consequently, the IPR remains quite high (~ 0.5) even
 283 at the resonance point as can be seen figure 1. At low
 284 frequency, this is valid for all momentum and parame-
 285 ter η , see figure 2.

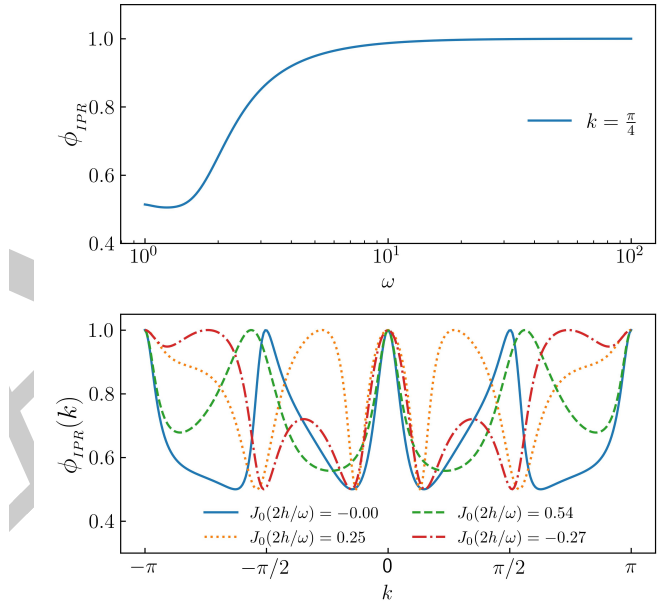


FIG. 2. Reduced IPR obtained by adiabatically increasing ω (top panel abscissa) for one the floquet mode obtained from equation 16 at the root of $J_0(\eta)$ for $N = 500$. IPR is ~ 0.5 (localized yet not fully freezing) upto $\omega \sim 2$, afterthat, smoothly increased to unity (fully localized and freezibg) at higher $\omega \geq 10$ (top panel, ordinate). At bottom panel cross-sections for four chosen amplitudes at $\omega = 2$ are plotted for a brillouin zone (abscissa) with corresponding reduced IPRs(ordinate).

288 Because the dependence of observable expectations
 289 on the eigenstates is always fairly strong for inte-
 290 grable systems like the TFIM, such systems will never
 291 exhibit any kind of thermal behaviour unless integra-
 292 bility breaking terms (such as strong disorder) are in-
 293 cluded [6]. As a result, it is not physically meaningful
 294 to refer to the unit IPR region as "Many Body Localiza-
 295 tion", because the parameter space lacks a thermal-

²⁹⁶ ized region to contrast with this state. The type of Flo-
²⁹⁷ quet Engineering described above, on the other hand,
²⁹⁸ can be easily applied to a broad class of nonintegrable
²⁹⁹ systems where FETH is expected to hold in certain re-
³⁰⁰ gions. Long-range spin systems, in particular, where
³⁰¹ the exchange energies between far-off spins are taken
³⁰² into account in the model Hamiltonian, are good can-
³⁰³ didates because they are known to thermalize when
³⁰⁴ driven with low frequencies [39].

305 II. LONG RANGE INTERACTIONS: THE LIPKIN 306 MESHKOV GLICK MODEL:

³⁰⁷ The periodically driven Curie-Weiss model for N
³⁰⁸ long-range spins is described by the Hamiltonian

$$\hat{H}(t) = \hat{H}_0 + [h \cos(\omega t) + h_0] \hat{H}_1. \quad (17)$$

³⁰⁹ Here, the undriven part \hat{H}_0 and the driven part \hat{H}_1 are,
³¹⁰ respectively,

$$\begin{aligned} \hat{H}_0 &= \frac{1}{2} \sum_{ij} J_{ij} \hat{\sigma}_i^z \hat{\sigma}_j^z, \\ \hat{H}_1 &= \sum_{i=1}^N \hat{\sigma}_i^x. \end{aligned} \quad (18)$$

³¹¹ The Heisenberg exchange energy of the bond between
³¹² spins i and j is given by

$$J_{ij} = \frac{J_\alpha}{N^{1-\alpha}} \frac{1}{r_{ij}^\alpha}, \quad (19)$$

with r_{ij} representing the smallest graph distance between them. Putting $\alpha = 0$ yields the Lipkin Meshkov Glick (LMG) model with all-to-all interactions $J_{ij} = J_0/N \forall(i, j), i \neq j$. We choose to maintain the extensivity of the interaction energy by enforcing the condition

$$\frac{J_0}{N} \sum_{i \neq j} 1 = \frac{J_0}{N} \frac{N(N-1)}{2} = 1,$$

³¹³ yielding the Kac-norm $J_0 = 2/(N-1)$. The
³¹⁴ Hamiltonian in equation 17 commutes with $P_{ij} \equiv$
³¹⁵ $\frac{1}{2}(1 + \vec{\sigma}_i \cdot \vec{\sigma}_j)$. In addition, it also commutes with
³¹⁶ the total angular momentum $S^2 = |\vec{S}|^2$, where $\vec{S} =$

³¹⁷ $S^x \hat{x} + S^y \hat{y} + S^z \hat{z} \equiv \frac{1}{2} \sum_i \vec{\sigma}_i$. We now choose to pop-
³¹⁸ ulate the system in a state with $S^2 = \frac{N}{2} \left(\frac{N}{2} + 1 \right)$.
³¹⁹ In that case, the dynamics remains invariant in the
³²⁰ $N+1$ -dimensional space spanned by the common
³²¹ eigen states of $P_{ij}, |S|^2$ and S_z ; the so-called *Totally*
³²² *Symmetric Subspace*, or TSS [40]. Let the eigenvalues
³²³ of S^z in the TSS be s_n , and the eigen vectors be $|s_n\rangle$.
³²⁴ Here, $s_n = -\frac{1}{2} + \frac{n}{N}$ and the index $n = 0(1)N$ has $N+1$
³²⁵ values. The dynamics is restricted to this invariant
³²⁶ subspace, wherein the matrix elements of the Hamil-
³²⁷ tonian are given by

$$\begin{aligned} \langle s_i | \hat{H}_0 | s_j \rangle &= -\frac{4}{N-1} s_i^2 \delta_{ij}, \\ \langle s_i | \hat{H}_1 | s_j \rangle &= \left[\sqrt{\frac{N}{2} \left(\frac{N}{2} + 1 \right) - N s_i (N s_{i+1}) \delta_{i+1,j}} \right. \\ &\quad \left. + \sqrt{\frac{N}{2} \left(\frac{N}{2} + 1 \right) - N s_i (N s_{i-1}) \delta_{i-1,j}} \right] \end{aligned} \quad (20)$$

³²⁸ These allow for a numerical representation of the
³²⁹ Hamiltonian in the TSS.

³³⁰ Next, we transform the Hamiltonian to the rotated
³³¹ frame given by the operator

$$\hat{U}(t) = \exp \left[i \frac{h}{\omega} \sin(\omega t) \hat{H}_1 \right]. \quad (21)$$

³³² This is analogous to the rotation performed for the
³³³ TFIM in eqns 10 and 11. Defining $\tau = \frac{h}{\omega} \sin \omega t$, we use
³³⁴ the fact that $\hat{H}_1 = 2S^x$, as well as the following iden-
³³⁵ tity obtained by using the Baker-Campbell-Hausdorff
³³⁶ formula,

$$e^{i2\tau \hat{S}^x} \hat{S}^z e^{-i2\tau \hat{S}^x} = \hat{S}^z \cos(2\tau) + \hat{S}^y \sin(2\tau), \quad (22)$$

to simplify the transformed Hamiltonian $\tilde{H}(t) = \hat{U}^\dagger(t) \hat{H}(t) \hat{U}(t) - \hat{U}^\dagger(t) \partial_t \hat{U}(t)$, yielding

$$\begin{aligned} \tilde{H}(t) &= -\frac{1}{N-1} \left[(S^z)^2 (1 + \cos 4\tau) + (S^y)^2 (1 - \cos 4\tau) \right. \\ &\quad \left. + \{S^y, S^z\} \sin 4\tau \right] - 2h_0 S^x. \end{aligned} \quad (23)$$

³³⁷ Next, we define $\eta \equiv 4h/\omega$ and use the Jacobi-Anger
³³⁸ formula in eqn 12 to expand $\tilde{H}(t)$. Ignoring constant
³³⁹ terms, this yields

$$\tilde{H}(t) \sim \frac{(\hat{S}^x)^2}{N-1} - 2h_0\hat{S}^x - \frac{J_0(\eta)}{N-1} \left[(\hat{S}^z)^2 - (\hat{S}^y)^2 \right] - \frac{2}{N-1} \sum_{k=1}^{\infty} J_{2k}(\eta) \left[(\hat{S}^z)^2 - (\hat{S}^y)^2 \right] \cos(2k\omega t) - \frac{2}{N-1} \sum_{k=1}^{\infty} J_{2k-1}(\eta) \{ \hat{S}^y, \hat{S}^z \} \sin[(2k-1)\omega t]. \quad (24)$$

340 If ω is large enough to smooth out the harmonic components, we obtain the RWA,
 341

$$\tilde{H}(t) \approx \tilde{H}_{\text{RWA}} \equiv \frac{(\hat{S}^x)^2}{N-1} - 2h_0\hat{S}^x - \frac{J_0(\eta)}{N-1} \left[(\hat{S}^z)^2 - (\hat{S}^y)^2 \right]. \quad (25)$$

342 If the drive amplitude h is adjusted such that η lies
 343 at a root of $J_0(\eta)$ (the localization point), the RWA
 344 Hamiltonian is diagonal in the representation of the
 345 transverse field \hat{S}^x , yielding an IPR of unity in that
 346 representation, similar to the TFIM in the previous
 347 section. Note however, that if the DC transverse field
 348 h_0 is set to 0, then, at the localization point, the RWA
 349 Hamiltonian $\tilde{H}_{\text{RWA}} \sim (\hat{S}^x)^2$. The eigenvalues are two-
 350 fold degenerate. This produces infinitely many (Flo-
 351 quet) eigenmodes in the degenerate subspace whose
 352 IPRs may not always be unity in the S^x representa-
 353 tion. The removal of this degeneracy necessitates the
 354 inclusion of the d.c. field h_0 . However, note that ratio-
 355 nal values of h_0 may add accidental degeneracies in
 356 \tilde{H}_{RWA} . To see this, note that, at a localization point,
 357 the eigenvalues of \tilde{H}_{RWA} in the TSS are given by

$$\text{Eigs}[\tilde{H}_{\text{RWA}}] = \frac{\left(\frac{N}{2} - m\right)^2}{N-1} - 2h_0 \left(\frac{N}{2} - m\right), \quad (26)$$

358 where the half-integer $-N/2 \leq m \leq N/2$ is the eigen-
 359 value corresponding to a particular eigenstate $|m\rangle$ of
 360 the symmetry-breaking field \hat{S}^x . In order to ensure
 361 that no additional degeneracies occur, we have to set
 362 h_0 in such a way that no two energies accidentally co-
 363 incide. If $N \gg 1$ (substantially large), then this con-
 364 dition can be readily met by assuring that $(1 - 2h_0)^{-1}$
 365 is never an integer that is divisible by N . To ensure
 366 this in our numerical simulations, we have kept h_0 at
 367 a small irrational value.
 368

369 The localization of the Floquet states at resonance is
 370 supported by exact numerical results, as can be seen
 371 in fig 3. Here, we show plots of the IPR of the Floquet
 372 modes $|\phi^n\rangle$ for $S^2 = (N/2)(N/2 + 1)$. The IPR in S^x
 373 representation is

$$\phi_{\text{IPR}}(n) = \sum_m |\langle m | \phi^n \rangle|^4. \quad (27)$$

374 These plots were obtained numerically by diagonaliz-
 375 ing the propagator $U(t)$ at $t = T$, where $U(t)$ is defined

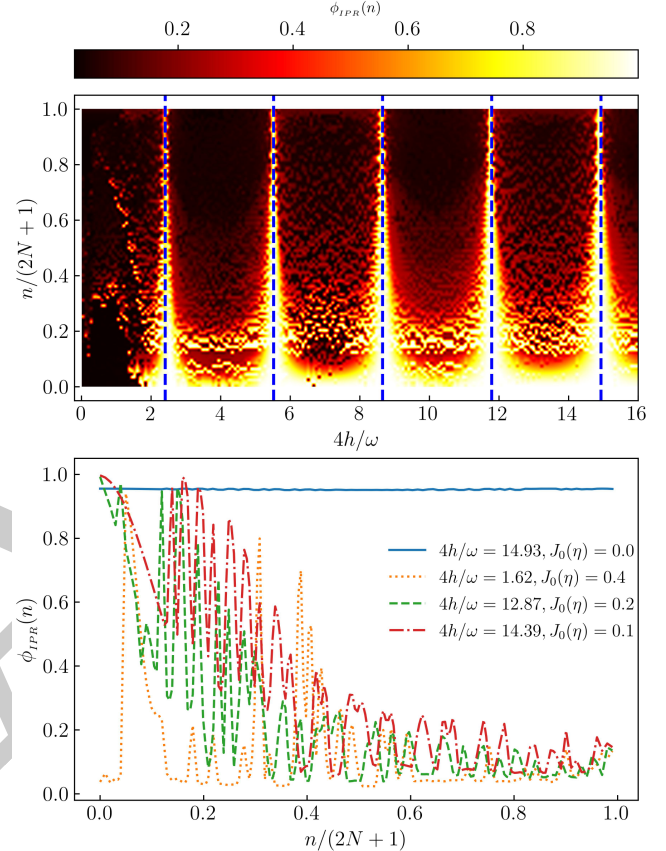


FIG. 3. IPR density plot for all possible Floquet modes (top panel ordinate) for different values of $\eta = 4h/\omega$ (top panel abscissa), deduced from equation 27 for exact LMG Hamiltonian for $N = 50$. Blue dashed lines are roots of $J_0(\eta)$. At bottom panel cross-section of IPR (ordinate)for four different η 's plotted for all possible floquet modes(bottom panel, abscissa) at $\omega = 90$. IPR founds to be \sim unity for all floquet modes at roots of J_0 .

376 in eqn 5. This propagator was obtained from simu-
 377 lations of the exact quantum dynamics using QuTiP,
 378 the Quantum Toolbox in Python [41]. We kept the fre-
 379 quency at a fairly large value $\omega = 90$ where we expect
 380 that RWA would be valid, and $N = \mathcal{O}(10^2)$. The density
 381 plot in the upper panel of fig 3 depicts the IPR of the
 382 Floquet states; the abscissa $\eta = 4h/\omega$ and the ordinate
 383 is $n/(2N+1)$, where $n \leq 2N$ is a nonnegative integer
 384 that indexes the Floquet states in increasing order of

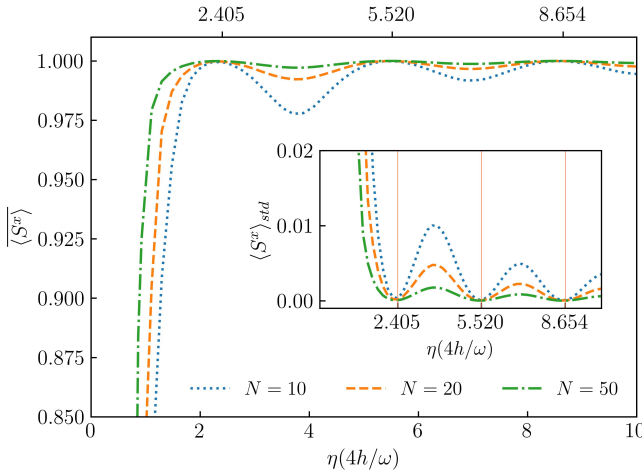


FIG. 4. Temporal average of $\langle \hat{S}^x \rangle$ (ordinate) for different η 's (abscissa) is plotted for $\sim 200T$ at higher ω for different $N=10,20,50$. $\langle \hat{S}^x \rangle$ is found to be unity at roots of $J_0(\eta)$. At points away from resonance points, $\langle \hat{S}^x \rangle$ falls below unity. The corresponding standard deviation $\langle \hat{S}^x \rangle_{std}$ supports the variation of $\langle \hat{S}^x \rangle$ (inset fig.). $\langle \hat{S}^x \rangle_{std}$ is ~ 0 describing a full freezing of the system at roots of $J_0(\eta)$ (red vertical solid lines).

³⁸⁵ m . The dashed vertical lines correspond to the roots ³⁸⁶ of $J_0(\eta)$. Comparing with the IPR of the TFIM in fig 1, ³⁸⁷ we can see a very similar patterns in the immediate ³⁸⁸ neighbourhood of the roots. Evidently, the IPR ap- ³⁸⁹ proaches a value of one for sufficiently large values of ³⁹⁰ the roots, strongly suggesting full DMBL. Deviations ³⁹¹ occur at the smallest root of $J_0(\eta)$ (around $\eta = 2.405$) ³⁹² due to the contributions from higher order terms in ³⁹³ eq 24. Thus, a higher root is favored for DMBL.

³⁹⁴ The bottom panel of fig 3 contains cross sections ³⁹⁵ of the full IPR plot for selected values of η as indi- ³⁹⁶ cated in the legend. When the drive amplitude h is ³⁹⁷ adjusted such that η is close to a root of $J_0(\eta)$, the Flo- ³⁹⁸ quet States are mixed, but not entirely thermal, since ³⁹⁹ the IPR does not fall to $\mathcal{O}(N^{-1})$, indicating that loca- ⁴⁰⁰ lization persists to some extent. However, the further ⁴⁰¹ we are from the roots, the closer the IPR gets to one ⁴⁰² predicted by thermalization.

⁴⁰³ Figure 4 shows plots of the long-time average (from ⁴⁰⁴ $t = 0 - 200T$) of the field amplitude $\langle \hat{S}^x \rangle$ as a function ⁴⁰⁵ of η . The system is started from the fully polarized ⁴⁰⁶ state $s_n = N/2$ in the TSS and the dynamics simulated. ⁴⁰⁷ The average is plotted for different values of ampli- ⁴⁰⁸ tude h , keeping the frequency fixed at a high value of ⁴⁰⁹ $\omega = 90$. It is clearly very close to unity at roots of $J_0(\eta)$ ⁴¹⁰ and falls at points away from it, indicating that S^x is ⁴¹¹ approximately conserved at the localization points.

⁴¹² Small deviations do occur due to the role of higher

⁴¹³ order terms in the rotated Hamiltonian in eq 23. This ⁴¹⁴ can be demonstrated quantitatively by comparing the ⁴¹⁵ IPR obtained from the exact dynamics simulation with ⁴¹⁶ that obtained from the dynamics of $\tilde{H}(t)$ in eq 23 after ⁴¹⁷ truncating the series at orders $k \geq 1$. This compari- ⁴¹⁸ son can be seen in fig 5. The IPR plots from the ex- ⁴¹⁹ act dynamics indicate that the first localization point, ⁴²⁰ represented by the lowest root of $J_0(\eta)$, does not show ⁴²¹ complete DMBL. However, DMBL is particularly con- ⁴²² spicuous at large roots. The IPRs of the Floquet states ⁴²³ obtained from the RWA dynamics exhibit large devia- ⁴²⁴ tions from unity when away from the localization point ⁴²⁵ as evidenced by the green and red curves in the mid- ⁴²⁶ dle panel of fig 5. However, complete localization is ⁴²⁷ seen in the RWA dynamics at any localization point, in ⁴²⁸ contrast to the exact case in the top panel. Thus, it ⁴²⁹ is necessary to incorporate higher-order corrections ⁴³⁰ into the Rotating Wave Approximation (RWA) at lower ⁴³¹ localization points. The application of the first-order ⁴³² correction to RWA in the lower panel of fig 5 results in ⁴³³ a curve structure that is closer to that from the exact ⁴³⁴ dynamics.

III. PERSISTENCE OF DMBL IN THE CONTINUUM LIMIT

⁴³⁸ In the continuum limit, where $N \rightarrow \infty$, the dispar- ⁴³⁹ ity between neighboring values of s_i in equation 20 ⁴⁴⁰ can be disregarded, and s_i can be mapped to a contin- ⁴⁴¹ uum $q \in [-1/2, 1/2]$ [40]. We define the Hamiltonian ⁴⁴² per particle $h(t) \equiv \frac{\dot{H}(t)}{N}$, and a canonically conjugate ⁴⁴³ co-ordinate $p \equiv \langle -i/N \frac{\partial}{\partial q} \rangle$. Then, in this limit, the ⁴⁴⁴ dynamics can be approximated by that of a classical ⁴⁴⁵ Hamiltonian [42]

$$h(t) = -2q^2 - [h \cos \omega t + h_0] \sqrt{1 - 4q^2} \cos p, \quad (28)$$

which yields the dynamical system

$$\begin{aligned} \frac{dq}{dt} &= \frac{\partial h}{\partial p} = h(t) \sqrt{1 - 4q^2} \sin p \\ \frac{dp}{dt} &= -\frac{\partial h}{\partial q} = 4q \left[1 - \frac{h(t) \cos p}{\sqrt{1 - 4q^2}} \right]. \end{aligned} \quad (29)$$

⁴⁴⁶ We have profiled simulations of the ensuing dynam- ⁴⁴⁷ ics with the Poincaré surface of section (PSOS) of the ⁴⁴⁸ full dynamics. Here, the (q, p) -phase space is strobed ⁴⁴⁹ at $t = nT$, and plotted for a large number of initial ⁴⁵⁰ conditions. The results are shown in the upper pan- ⁴⁵¹ ells of fig 6 for a small value of $\omega = 2.5$ (left panel) ⁴⁵² and a large value $\omega = 90$ (right panel). In both cases, ⁴⁵³ the value of h is chosen such that η lies on the first ⁴⁵⁴ root of $J_0(\eta)$. The onset of chaos for small drive fre- ⁴⁵⁵ quency indicates thermal behaviour for typical initial ⁴⁵⁶ conditions, with small islands of regularity for others.

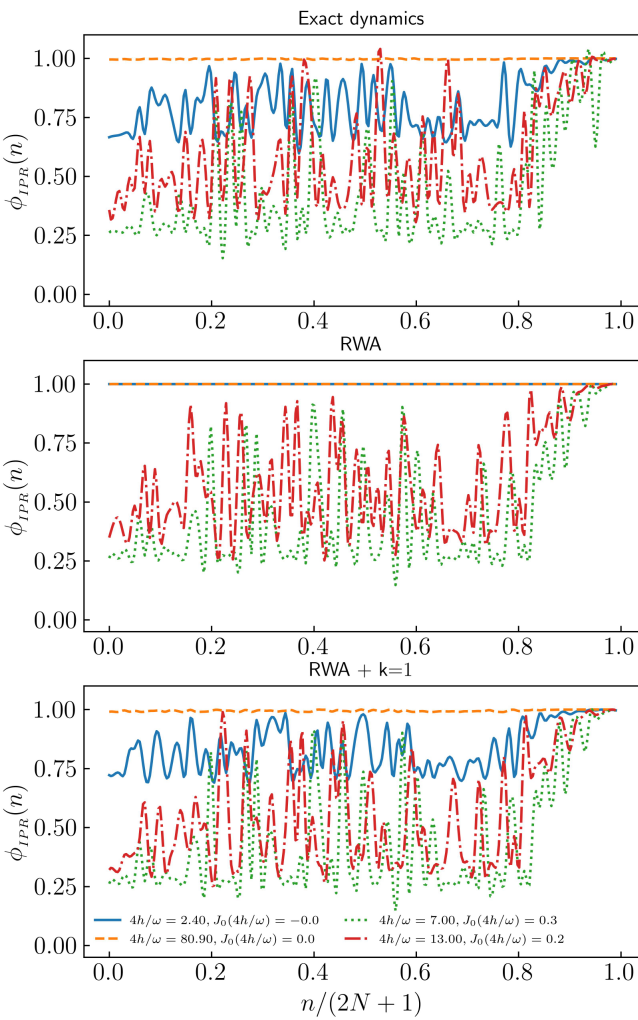


FIG. 5. The comparison between IPR for exact dynamics and RWA with corresponding correction orders. IPR is calculated for four different η 's and corresponding $J_0(\eta)$ values for colors, Blue: $\eta = 2.40, J_0(\eta) = 0.0$, dashed orange: $\eta = 80.9, J_0(\eta) = 0.0$, Green: $\eta = 7.0, J_0(\eta) = 0.3$, Red: $\eta = 13, J_0(\eta) = 0.2$. At low root of $J_0(\eta)$ IPR is not unity (Blue curve) where at higher root (orange dashed) it is unity while at points away from roots IPR are less than unity in the exact (top panel) plot. RWA does not matches with the exact plot. At all roots of $J_0(\eta)$ IPR is unity(middle panel). RWA with additional higher order terms exhibit similar system pattern(Bottom panel) with exact dynamics.

This is consistent with similar results for small frequencies reported in [39, 43]. However, at high frequency, the regular islands distinctly dominate over the chaos. The trajectories indicate that the conser-

vation of $\langle S^x \rangle \approx \sqrt{1 - 4q^2} \cos p$ [40] at high ω persists in the thermodynamic limit. That this is a signature of the underlying quantum dynamics can be readily seen in the quantum phase space representation of the Floquet Eigenstates for a large but finite N . These are shown in the corresponding lower panels of fig 6. Here, we have plotted the Spectral Average of the Husimi Q-functions of the acquired Floquet States in the TSS. Specifically, for a coherent state $|q, p\rangle$, the corresponding Spectral-Averaged Husimi distribution [44] is obtained by

$$H(q, p) \equiv \frac{1}{(2N+1)\pi} \sum_n \langle q, p | \phi^n \rangle \langle \phi^n | q, p \rangle \quad (30)$$

The quantum phase space retains signatures of the classical phase space dynamics when $N = 500$, indicating the onset of the persistence of S^x conservation that arises from the resonance condition at high frequencies.

IV. PHASE CROSSOVER FROM THERMAL TO DMBL

The analysis of the periodically driven LMG model reveals two distinct scenarios at low and high external drive frequencies. In the former case, thermalization in accordance with FETH is seen, whereas in the latter case, DMBL is induced. As a result, we hypothesize that a macroscopic change in phase occurs due to the influence of frequency.

To demonstrate this, we investigate the IPR of the Floquet mode with smallest quasienergy for numerous frequencies and system sizes, along with the associated drive amplitude h keeping the system at a localization point. The results are shown in fig 7. In the low-frequency range $\omega \in [1.0, 9.0]$, the IPR exhibits values well below unity. Moreover, the IPR gradually diminishes with increasing system size, following a system size inverse proportional trend, which confirms the participation distribution (as shown in the bottom panel). As the limit $N \rightarrow \infty$, the inverse participation ratio (IPR) tends towards zero, indicating a fully delocalized state. The plots reveal a gradual increase in the unity of IPR over a certain frequency range, specifically at $\omega \approx 5.0$. In addition, the rise does not cross with those for different values of N , suggesting the onset of a phase crossover [27, 45]. As the size of the system increases, the crossover region becomes smoother, rather than sharper.

We can also look at this crossover more clearly in the plots of the heating rate of the system, defined simply by the expectation value of the Hamiltonian, $\langle \hat{H}(t) \rangle$. We have carried out the numerical evaluation from the simulated dynamics over $t = 500T$. When the system is adequately described by FETH,

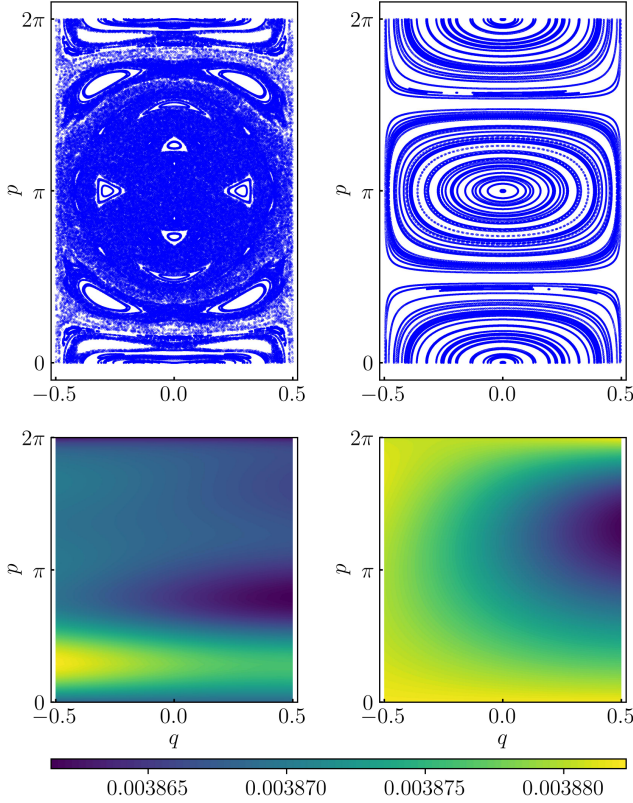


FIG. 6. Phase-space distributions at $\omega = 2.5$ (left panels) and $\omega = 90.0$ (right panels) for 100 initial conditions. At small ω , the classical PSOS, obtained from simulating the dynamics in eqns 29 (top left panel), shows chaotic behaviour, whereas at the higher ω , the onset of regular dynamics can be readily seen (top right panel). The bottom panels plot the corresponding Spectral-Averaged Husimi-Q function, obtained from the Floquet modes $|\phi^n\rangle$ using eqn 30. The $\omega = 2.5$ -case (bottom left panel) has a uniform distribution with less contrast in colour. This is consistent with the chaotic behaviour seen in the continuum limit. In the $\omega = 90$ -case (bottom right panel), the distribution has distinct colour contrasts, which is consistent with the regular dynamics pattern seen in the continuum limit.

the temporal fluctuations in the heating rate, defined by $\langle H \rangle_{std}^2 \equiv \overline{\langle \hat{H} \rangle^2} - \overline{\langle \hat{H} \rangle}^2$ (see eqn 3), are minimal in the thermodynamic limit, as the spread of states leads to a limited standard deviation[46]. Conversely, the onset of athermal behavior is indicated by nonzero fluctuations in time. If we set the initial state to the fully polarized state in the TSS (given by $|s_N\rangle$), then the onset of freezing, together with DMBL, will result in nearly infinite hysteresis in the ensuing dynamics, causing $|\psi\rangle(t) \approx |s_N\rangle \forall t$. From eqn 17, we can clearly see that this will lead to a linearly rising dependence on ω in

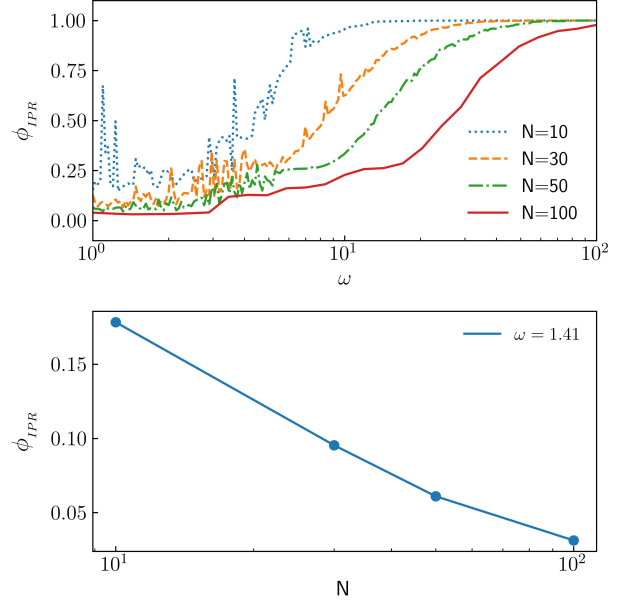


FIG. 7. IPR is plotted (top panel, ordinate) for a range of $\omega \in [1, 100]$ (top panel, abscissa) for four different $N = 10, 30, 50, 100$ at root of $J_0(\eta)$. At small ω upto $\omega \sim 10$ IPR founds to be very small and rises slowly upto unity (fully localized) at higher frequencies. At bottom panel IPR (ordinate) is plotted for different $N = 10, 30, 50, 100$ (bottom panel, abscissa) for a random small $\omega \sim 1$ at root of $J_0(\eta)$ from the values from top panel. IPR falls as proportional to inverse of N 's value which is a fully distributed state. The smooth rise in IPR defines a phase cross over (top panel) between a fully distributed thermal phase to a fully localized freezing phase.

⁵²³ $\langle H \rangle_{std}$ as long as we stick to a localization point given
⁵²⁴ by a fixed h/ω . All these observations are corroborated by the heating rate plots in figure 8.

Review from here

V. OBSERVATIONS AND DISCUSSION

529 DMBL is investigated in TFIM at different drive frequencies and corresponding amplitudes, where the system localization-resonance points are found to be the roots of $J_0(2h/\omega)$ for both exact and RWA. The delocalization away from resonance points is relatively weak due to integrability of the Ising model which allows for localization to persist. This is consistent also at adiabatically varied TFIM at resonance point where system never goes thermal even at the smallest possible ω . The LMG model exhibits distinct localization at resonance points which are roots of $J_0(4h/\omega)$. However, there is some degree of delocalization observed beyond these points, albeit weak. The non-integrability of the LMG model and the established onset of chaos in the thermodynamic limit at low ω

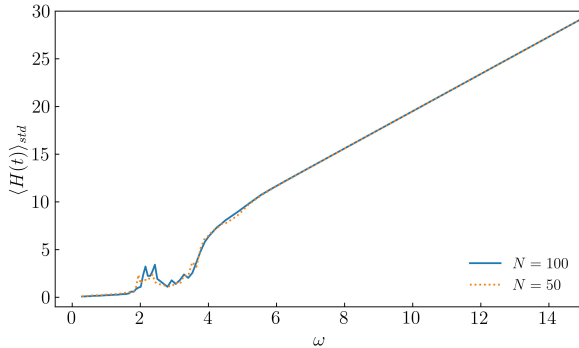


FIG. 8. The standard deviation of the heating rate, denoted by $\langle H \rangle_{std}$, calculated over a span of $t = 500T$ for two system sizes. Here, h is varied to keep $\eta = 4h/\omega$ at the first root of $J_0(\eta)$. A nonsingular rise has been identified at $\omega \approx 4.0$. $\langle H \rangle_{std}$ exhibits a diminutive magnitude below that value of ω , while a linear rise is observed at higher frequencies, consistent with freezing. A vanishingly small standard deviation for $\omega \ll 4.0$ indicates the presence of a thermal region, whereas a larger finite standard deviation suggests the existence of athermal behaviour. The small peaks observed at $\omega \in [2, 4]$ are finite-size effects that disappear in the thermodynamic limit.

lead to a near-complete thermalization in IPR of the Floquet states at small ω 's. Additionally, we adiabatically varied ω, h in the LMG model at resonance point where a smooth crossover from thermal to localized phase is observed fig.7. At low frequencies, IPR is found to decrease with increasing system size N . At large $N \rightarrow \infty$, IPR goes down to zero resulting in a system fully thermalized. This is in contrast to the TFIM, which lacks such a change in phase. Thus, the incorporation of LMG appears to cultivate a change in phase from the thermal phase to the localised phase, a property that can be utilized in designing an MBL engine.

VI. CONCLUSION AND OUTLOOK

This article delved into the onset of freezing and phase cross-over in 1D fermionic spin systems driven by transverse periodic field, focusing TFIM and LMG model paradigmatic examples. The parametrization of DMBL is based on IPR of the Floquet eigenstates. The present study conducted a numerical comparison between IPRs of the LMG model and TFIM at both low and high drive frequency domains. We found the emergence of thermal behavior at low frequencies and freezing at high frequencies, as well as the appearance of additional approximately conserved quantities.

Conclusion: Long-range spins exhibit strong localization in spin-coordinate space for the LMG model when the drive frequency is $\omega \gg J$, where J represents the spin exchange energy. The localization of the LMG model occurs at specific resonance points of the drive frequency ω and amplitude h , at $J_0(4h/\omega) = 0$. The TFIM case has shown comparable localization (in momentum space) at resonance points, determined by $J_0(2h/\omega)$. However, the mechanism differs in long-range systems as a distinct observable (S_x) is conserved in the LMG case, where S represents the total spin. Upon the removal of accidental degeneracy through the application of a DC transverse field in the form of $\sim \hat{S}_x$, the eigenstates can be mapped into a coordinate representation, leading to a robust spatial localization. The adiabatically increased periodic drive frequency in driven LMG model exhibits smooth increase in IPR yielding a quantum phase-crossover from thermal to localized phase. The absence of thermal behavior in the low-frequency limit of the short-range transverse field Ising model (TFIM) can be attributed to the significant magnitude of the inverse participation ratio (IPR). The emergence of thermal and localized states in long-range systems can be achieved through Floquet engineering, in the absence of disorder.

Outlook: A set of clean non-equilibrium quantum systems characterized by high symmetry has been thoroughly investigated. Akin to TFIM, the onset of thermalization in LMG can be postponed when the condition $\omega \gg J$ and $J_0(4h/\omega) = 0$ is satisfied. In systems possessing a Hamiltonian of the form given by equations 18 and 19, the time-independent Schrödinger equation can be solved analytically for certain potentials. The intermediate spin-spin interaction power law limits have received less attention compared to the infinite and long-range limit. Further research can be conducted on this topic. The LMG spin configuration undergoes a phase cross-over due to the adiabatic increase in drive frequency. This suggests the possibility of a future MBL engine that can operate between the thermal and localized regimes, with a thermodynamic cycle. Additionally, there exist prospects for diabatic corrections.

Acknowledgement: One of the authors, MR would like to acknowledge The University of Burdwan for support via a state-funded fellowship, as well as for providing computational resources. AR acknowledges support from the University Grants Commission (UGC) of India, via BSR Startup Grant No. F.30-425/2018(BSR), as well as from the Science and Engineering Research Board (SERB) Core Research Grant No. CRG/2018/004002.

-
- 624 [1] P. Bordia, H. Lüschen, U. Schneider, M. Knap, and 666 [24] M. Bukov, L. D'Alessio, and A. Polkovnikov, ArXiv:
 625 I. Bloch, *Nature Phys.* **13**, 460.
 667
 626 [2] S. Sahoo, I. Schneider, and S. Eggert, Periodically 668 [25] L. D'Alessio and M. Rigol, *Phys. Rev. X* **4**, 041048
 627 driven many-body systems: A floquet density matrix 669 (2014).
 628 renormalization group study (2019), arXiv:1906.00004 670 [26] R. Yousefjani, S. Bose, and A. Bayat, *Phys. Rev. Res.* **5**,
 629 [cond-mat.str-el]. 671 013094 (2023).
 630 [3] A. Das, *Phys. Rev. B* **82**, 172402 (2010). 672 [27] P. Sierant, M. Lewenstein, A. Scardicchio, and J. Za-
 631 [4] G. B. Mbeng, A. Russomanno, and G. E. Santoro, The 673 krzewski, *Phys. Rev. B* **107**, 115132 (2023).
 632 quantum ising chain for beginners, arXiv:2009.09208.
 633 [5] H. S. Yamada and K. S. Ikeda, *Phys. Rev. E* **105**, 674 [28] S. Rozhin, Abolfazl 10.1103/PhysRevRe-
 634 054201. 675 search.5.013094.
 635 [6] A. Roy and A. Das, *Phys. Rev. B* **91**, 121106. 676 [29] L. N. Alet Fabien **19**, 10.1016/j.crhy.2018.03.003.
 636 [7] H. Li, B. Shapiro, and T. Kottos, *Phys. Rev. B* **98**, 677 [30] S. J. Garratt and S. Roy, *Phys. Rev. B* **106**, 054309.
 637 121101 (2018). 678 [31] R. B. Stinchcombe, *J. Phys. C: Solid State Phys.* **6**, 2459.
 638 [8] A. Eckardt and E. Anisimovas, *New J. Phys.* **17**, 093039 679 [32] F. E. H. George Arfken, Hans Weber, *Mathematical
 639 (2015). 680 Methods for Physicists*, 7th ed. (Academic Press).
 640 [9] L. Zhang, V. Khemani, and D. A. Huse, *Phys. Rev. B* **94**, 681 [33] S. Mukherjee, A. Spracklen, D. Choudhury, N. Gold-
 641 224202 (2016). 682 man, P. Öhberg, E. Andersson, and R. R. Thomson, *New
 642 [10] V. Khemani, A. Lazarides, R. Moessner, and S. Sondhi, 683 J. Phys.* **17**, 115002.
 643 *Phys. Rev. Lett.* **116**, 250401. 684 [34] S.-H. Lin, B. Sbierski, F. Dorfner, C. Karrasch, and
 644 [11] N. Yunger Halpern, C. D. White, S. Gopalakrishnan, and 685 F. Heidrich-Meisner, *SciPost Physics* **4**, 002.
 645 G. Refael, *Phys. Rev. B* **99**, 024203. 686 [35] N. C. Murphy, R. Wortis, and W. A. Atkinson, *Phys. Rev.*
 646 [12] A. Campa, T. Dauxois, and S. Ruffo, *Physics Reports* 687 **B** **83**, 184206.
 647 **480**, 57.
 648 [13] T. Eisele and R. S. Ellis, *J Stat Phys* **52**, 161.
 649 [14] A. Canning, *Physica A: Statistical Mechanics and its 688 [36] E. J. Torres-Herrera, I. Vallejo-Fabila, A. J. Martínez-
 650 Applications* **185**, 254.
 651 [15] D. Vu, K. Huang, X. Li, and S. Das Sarma, *Phys. Rev.* 689 Mendoza, and L. F. Santos, *Phys. Rev. E* **102**, 062126.
 652 *Lett.* **128**, 146601 (2022).
 653 [16] G. Misguich, V. Pasquier, and J.-M. Luck, *Phys. Rev. B* 690 [37] N. Trivedi and D. Heidarian, *Progress of Theoretical
 654 **94**, 155110 (2016). 691 Physics Supplement* **160**, 296.
 655 [17] M. Calixto and E. Romera, *J. Stat. Mech.* **2015**, P06029.
 656 [18] K. Fujii, *Journal of Modern Physics* **8**, 2042.
 657 [19] D. A. Abanin, E. Altman, I. Bloch, and M. Serbyn, *Rev. 692 [38] G. Misguich, V. Pasquier, and J.-M. Luck, *Phys. Rev. B*
 658 Mod. Phys.* **91**, 021001 (2019). 693 **94**, 155110.
 659 [20] M. Srednicki, *Phys. Rev. E* **50**, 888.
 660 [21] M. Srednicki, *Journal of Physics A: Mathematical and 694 [39] A. Russomanno, R. Fazio, and G. E. Santoro, *EPL* **110**,
 661 General* **32**, 1163 (1999). 695 37005.
 662 [22] M. Holthaus, *J. Phys. B: At. Mol. Opt. Phys.* **49**, 013001 696 [40] T. Mori, *J. Phys. A: Math. Theor.* **52**, 054001.
 663 (2016).
 664 [23] M. Vogl, M. Rodriguez-Vega, and G. A. Fiete, *Phys. Rev.* 697 [41] J. Johansson, P. Nation, and F. Nori, *Computer Physics
 665 **B** **101**, 024303 (2020). 698 Communications* **184**, 1234.
 699 [42] B. Sciolla and G. Biagioli, *Phys. Rev. Lett.* **105**, 220401.
 700 [43] R. A. Kidd, M. K. Olsen, and J. F. Corney, *Phys. Rev. A* 701 **100**, 013625 (2019).
 702 [44] A. Bäcker, S. Fürstberger, and R. Schubert, *Phys. Rev.* 703 **E** **70**, 036204 (2004).
 704 [45] S. Sachdev, *Quantum Phase Transitions*, 2nd ed. (Cam-
 705 bridge University Press, Cambridge, 2011).
 706 [46] P. Reimann, *J. Stat. Mech.* **2021**, 103106.